Chain-stretch relaxation from low-frequency Fourier transform rheology

C. D. Reynolds ⬤
Department of Chemistry, Durham University, Durham, DH1 3LE, United Kingdom
and Department of Metallurgy and Materials, University of Birmingham, Edgbaston, Birmingham, B15 2SE, United Kingdom

D. M. Hoyle ⬤
Department of Chemistry, Durham University, Durham, DH1 3LE, United Kingdom
and Offshore Renewable Energy Catapult, Blyth, Northumberland, NE24 1LZ, United Kingdom

T. C. B. McLeish ⬤
Department of Physics, Durham University, Durham, DH1 3LE, United Kingdom
and Department of Physics, University of York, Heslington, York YO10 5DD, United Kingdom

R. L. Thompson ⬤
Department of Chemistry, Durham University, Durham, DH1 3LE, United Kingdom

Medium- or large-amplitude oscillatory shear (MAOS and LAOS, respectively) is sensitive to polymer chain structure, yet poses unsolved challenges for *a priori* structural characterization. We present a MAOS protocol applied to near-monodisperse linear polymer melts, from which chain-stretch relaxation, a key structural feature, is discernible. The third harmonics of MAOS frequency sweeps are decomposed into real and imaginary components and found to obey time-temperature superposition. Significantly, these third harmonic features occur at low frequency and are readily accessible with standard rheometers. For materials where phase transitions restrict the use of time temperature superposition, this method has potential to greatly increase the scope of rotational rheometry for structural analysis of polymers. However, the relationship between MAOS data and characteristic relaxation times is complex, and to elucidate this, a modeling approach is required. The GLaMM molecular tube-based model of linear entangled melt rheology and structure, which has no free parameters, closely follows the form of our experimental results for the third harmonics and contains discriminatory features which depend only on the polymer's chain stretch relaxation time. However, we find fundamental differences in magnitude and the frequency dependence of the third harmonics which must be resolved in order to fully understand the molecular basis of the stress response and quantitatively study chain stretch.

I. INTRODUCTION

Oscillatory shear rheology is sensitive to the microstructure of complex soft materials (e.g., polymers [1–3] or immiscible blends [4]). The technique subjects a fluid sample to oscillatory shear strain at a given amplitude and frequency, $\gamma(t) = \gamma_0 \sin(\omega t)$, and analyzes the stress response. Medium- or large-amplitude oscillatory shear (MAOS and LAOS respectively, where MAOS is a special case of LAOS at intermediate strains) is defined as having γ_0 sufficient to induce detectable levels of nonlinear stress response (for a review see Hyun *et al.* [5]).

LAOS reveals microstructural information (additional to that available from linear rheology) in a range of viscoelastic

materials, e.g., gels and networks [6–8], wormlike micelles [9], soft glasses [10], emulsions [11], particle suspensions [12], and biological fluids [13].

For polymers in particular, LAOS is complementary to small-amplitude measurements, and results are a complex function of molecular architecture such as linear [14], star [15], and comb architectures [16] and can be used to quantify the level of branching in industrial resins such as metallocene-catalyzed sparsely branched HDPEs [17,18] or tubular-reacted randomly branched LDPEs [18,19]. However, crucially, LAOS is not yet a standard analytical tool for characterizing molecular architecture.

The stress response of a complex material in LAOS can be characterized in several ways. The transient shear stress can be plotted against time, and visual distortions from a sinusoidal curve can be seen [20]. However, the shear stress is more commonly plotted against strain to give Lissajous-Bowditch curves [21,22], and these are grouped together for various frequencies and strain amplitudes in Pipkin diagrams [13], which give a visual "fingerprint" of a material. For more quantitative analysis, the stress is typically decomposed into some series

such as Fourier [5], Chebyshev polynomials [13], or graphical interpretations [23]. It is worth noting that no dominant methodology is established as a benchmark analysis method.

In this paper we focus on Fourier transform rheology (FTR) because this has been shown to be a sensitive enough technique to isolate small nonlinearities in the material stress response, either from shear stress [5,24–27] or from the first normal stress [28].

In FTR the shear stress response to the imposed sinusoidal shear rate is expressed as a Fourier series, $\sigma_{xy}^{FT} = \sum_n [I_n' \sin(n\omega t) + I_n'' \cos(n\omega t)]$, where I_n' and I_n'' are the Fourier coefficients. The complex dynamic moduli for the nth harmonic are defined as $G_n' = I_n'/\gamma_0$ and $G_n'' = I_n''/\gamma_0$. For $n = 1$ we recover the standard storage and loss moduli: $G' = I_1'/\gamma_0$ and $G'' = I_1''/\gamma_0$ as $\gamma_0 \to 0$.

Nonlinearities in LAOS are measured typically through the third harmonics ($n = 3$) since by symmetry the even harmonics are zero [29] (we use the second harmonic to measure the noise).

Popular reported quantities are the absolute value of the third harmonic $I_3 = \sqrt{I_3' + I_3''}$ and its value as a ratio to the absolute first harmonic, $I_{3/1} = I_3/I_1$, which is often plotted as a function of increasing γ_0 [27]. Secondarily considered is the phase shift of the third harmonic $\Phi_3 = \phi_3 - 3\phi_1$, with $\tan(\phi_n) = \frac{G_n''}{G_n'}$ [18] and $Q = I_{3/1}\gamma_0^{-2}$, which plateaus to a constant value (Q_0) in the limit of small amplitude [30]. Q_0 can also be decomposed into Q_0' and Q_0'' [31].

Nonlinearities in the first harmonic have been used to characterize behavior at high strains [32] and to predict the form of the third harmonic [33]. However, we choose to focus on the third harmonic where nonlinearities occur at small strains and are experimentally accessible.

Of recent interest is the MAOS protocol (see, e.g., Ref. [29]), defined as the strain regime within which the imposed γ_0 is sufficient for nonlinearities in the stress to be experimentally measured yet maintain the relation $I_{3/1} \propto \gamma_0^2$.

Interpretation of LAOS-FTR results relies on comparison with some relevant constitutive theory, since this method does not explicitly reveal a direct relationship between material microstructure and the subsequent higher harmonic dependency (several are covered in Ref. [5]).

However, constitutive modeling of LAOS is comparatively underdeveloped. Hyun [34] compared several constitutive models such as the Giesekus, Phan-Tien Tanner, and Pompom model. An example using the Giesekus model is given in the Appendix. The model contains a nonlinearity factor (α) which can be fitted to the medium-amplitude oscillatory shear (MAOS) response but cannot capture all flows (transient shear, extension, and MAOS) with a single value. The Pom-pom model has been used to characterize branching [17,18,20], which has been effective due to its structure-based construction and parametrization. The molecular stress-function (MSF) theory has also been shown to be capable of capturing extensional and LAOS rheology simultaneously [19]. For the MAOS regime both the Pom-pom and MSF theories have been shown to broadly capture the intensity of $I_{3/1}$ over a range of frequencies for a range of materials from monodisperse linear and star-arm to randomly branched polymers [14,15,17].

TABLE I. Material parameters for the polyisoprene samples at a reference temperature of 25 °C.

Sample name	Mw [kg/mol]	PDI	η_0^* [Pa s]	τ_d [s]	Z
PI20k	21.5	1.02	126	0.000 58	5
PI100k	100	1.03	31 600	0.155	21
PI150k	145	1.02	113 000	0.55	30
PI400k	387	1.05	2 910 000	13.8	80

A limitation of all these approaches is that fitting is required to match theory to LAOS data; typically the parameters are set by a different rheometric experiment and the fits are "multimodal" in form. These factors obscure the true molecular response and hence the ability of the LAOS technique to inform on structure.

The aim of this paper is the following:

(1) To present the rich phase information that is contained in the third harmonic and show that this can be meaningfully used to characterize the molecular rheology of well-defined materials (including parameters that can be extremely difficult to obtain from linear rheology) and

(2) To compare these new results with theoretical modelling, both via a fitted multimodal approach and the most detailed truly molecular constitutive model currently available.

II. MATERIALS AND EXPERIMENTAL

Linear polybutadiene chains of defined molecular weights were synthesized by standard living anionic polymerization [35]. In Table I we detail the material parameters measured using gel permeation chromatography (GPC) and standard oscillatory rheology.

Rheological experiments were performed on a Discovery HR-2 (TA Instruments) equipped with an environmental test chamber supplied with liquid nitrogen. For linear rheology, a 25 mm parallel plate geometry was used, and the dynamic moduli were measured using frequency sweeps (10^{-2} Hz $\leqslant \omega \leqslant 10^2$ Hz and 1% $\leqslant \gamma_0 \leqslant$ 5%) at various temperatures between -30 °C and 50 °C. The results at each temperature were shifted to a reference temperature of 25 °C using WLF theory [36] and REPTATE software [37].

MAOS measurements were carefully made in seperate experiments using a 25 mm, 4° cone. Frequency sweeps were performed for strain amplitudes of 5% $\leqslant \gamma_0 \leqslant$ 20% and frequencies under 5 rad/s to limit inertial and instrument effects. Transient data were recorded, and the Fourier coefficients for the stress were extracted from the transient stress data using an in-house MATLAB program [38], which uses a fast Fourier transform routine.

Care was taken during sample preparation and measuring to ensure the accuracy of the LAOS results, with details of these protocols given in the Appendix and in Ref. [39].

III. MODELING

We compare the polyisoprene rheology to a self-consistent set of constitutive equations that transition from linear to nonlinear theory using the the same underlying concepts. First, the
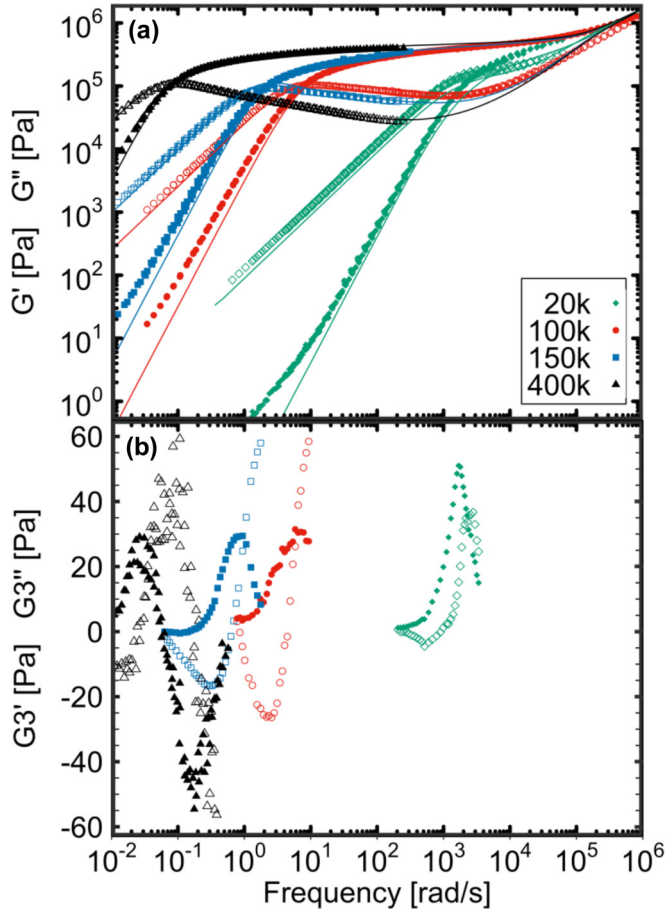
FIG. 1. (a) Linear rheology for the four PI blends at 25 °C detailed in Table I with comparison to Likhtman-McLeish linear theory. (b) MAOS rheology for the four blends at 25 °C with a strain of 20% where the open symbols are G'_3 and the closed = G''_3. For PI400k the results are a TTS for temperatures in the range of 25 °C–50 °C.

Likhtman-McLeish linear theory [40] accurately describes the full relaxation pathways of linear polymer chains subjected to a linear deformation. This theory is then extended to the GLaMM model [41,42], which considers nonlinear stress response of the whole chain using a series of well-considered approximations and closure assumptions. The GLaMM model offers a sophisticated treatment of monodisperse linear polymer melts that includes several relaxation mechanisms: chain diffusion, chain stretch, convective constraint release, and contour length fluctuations. Although the GLaMM model captures nonlinear rheology without the need for fitting free parameters, it is computationally expensive, and for simulations with any spatial variance in the flow rates, it is more convenient to use the coarse-grained version of the model: the Rolie-Poly [43] model. This considers the chain as a single end-to-end vector, as opposed to the contour dependence included in the GLaMM model. We consider both a one-mode model and a multimode model. The multimode version of the Rolie-Poly model is used to restore the transient features lost in removing higher frequency chain motion during coarse graining of the GLaMM model. However, the multimode Rolie-Poly model must be fitted either against GLaMM
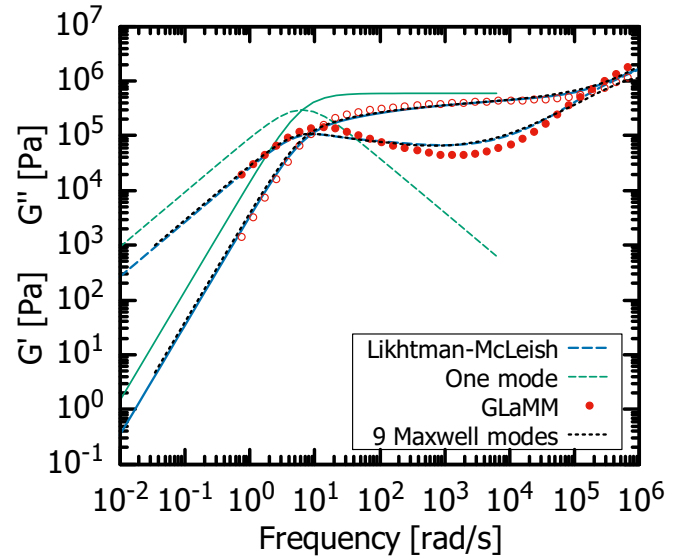

FIG. 2. Linear dynamic moduli predictions for PI100K at 25 °C, using Likhtman-McLeish theory, GLaMM, and Rolie-Poly with one and nine Maxwell modes. Details of the parameters used are provided in the Appendix.

predictions or experimental data for rheological linear and nonlinear flows.

IV. RESULTS

We consider the linear and nonlinear oscillatory shear for four molecular weights of polyisoprene. All the samples are entangled: with one sample weakly entangled (number of entanglements per chain, $Z = 5$), two samples moderately entangled ($Z = 21$ and $Z = 30$), and one sample highly entangled ($Z = 80$). Figure 1 shows the linear rheology of the
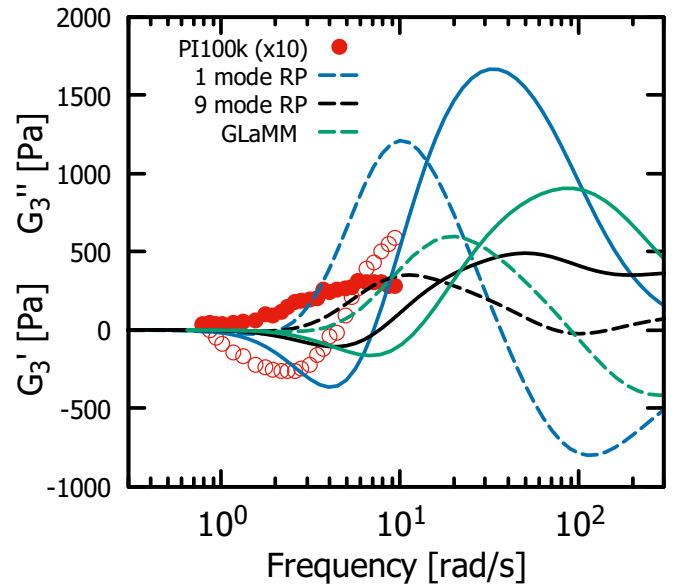

FIG. 3. GLaMM predictions of third harmonics compared to Rolie-Poly with one and nine modes and experimental results. The open symbols and solid lines are G'_3, and the filled symbols and dashed lines are for G''_3.
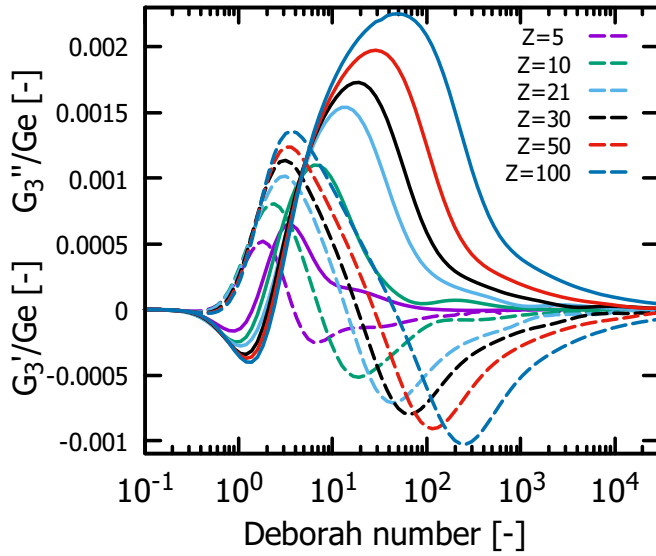
FIG. 4. GLaMM predictions of third harmonics with varied entanglement number. The solid lines are G_3', and the dashed lines are G_3''.

FIG. 5. Counterpart to Fig. 4. Variations in $G3'$ and $G3''$ as a function of Z with comparison to the dynamic moduli. Of particular note is the characteristic crossover frequencies for each set of harmonics. In contrast to the experimental data the crossover for the third harmonics occurs at a higher frequency than the standard crossover.

four materials at 25 °C with properties given in Table I. For all materials the terminal crossover was experimentally accessible giving the reptation relaxation time τ_d, and for PI20K and PI100k the high-frequency crossover was also measured, giving the entanglement relaxation time τ_e. The only characteristic difference between the samples is that the weakly entangled PI20k shows no minimum in G''. Also in this figure are the predictions of the Likhtman-McLeish linear theory, without adjustable parameters (lines), which gives an excellent prediction of the linear rheology for all four samples with the only parameter differentiating them being the molecular weight.

In the bottom half of Fig. 1 the real and imaginary parts of the third harmonic are plotted for each PI sample. PI20k–PI150k were measured at 25 °C with a strain of 20% and PI400k at higher temperatures (up to 50 °C) transposed to 25 °C with time-temperature superpostion. All sets of curves follow similar qualitative behavior, with shifts in frequency with molecular weight in a manner that tracks the linear rheology. The key feature of the third harmonic curves is a crossover in G_3' and G_3'', which is always found at a lower frequency than the crossover associated with the terminal relaxation time in the linear rheology (and orders of magnitude lower than the frequency equal to the inverse chain stretch time). For the moderately and highly entangled polymers, the crossover occurs close to the peak value of G_3' and the inflection point of G_3''. However, the weakly entangled PI20k has a different shape, with G_3' rising to a higher maxima before falling to crossover at the lower peak value of G_3''. A plot of Fig. 1 with frequency normalized by τ_d (see Fig. 6) and details of the TTS of PI400k are given in the Appendix.

V. DISCUSSION

The LAOS results in Fig. 1 show several nonlinear features including a crossover between G_3' and G_3'', and extrema in both. These features move to lower frequencies with increasing Mw. Plotting the results against Deborah number
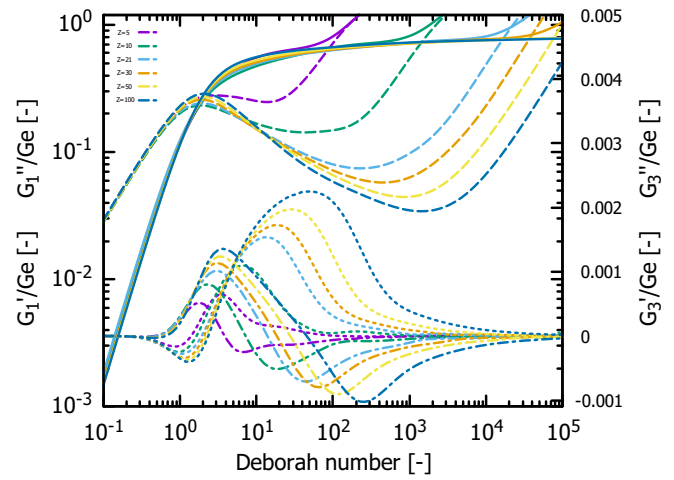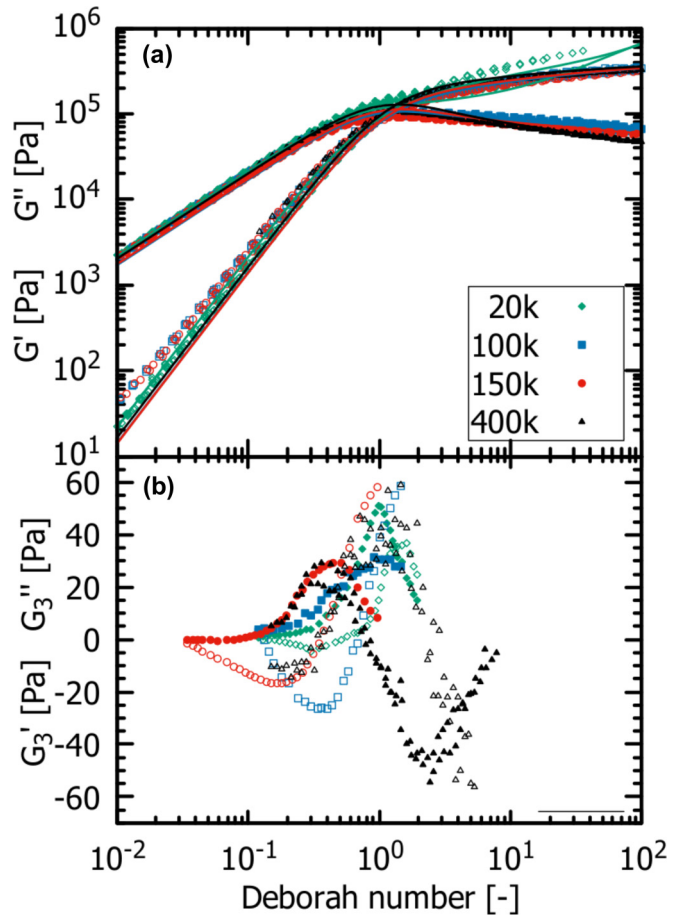

FIG. 6. The analog to Fig. 1 plotted as a function of Deborah number (frequency normalized by terminal relaxation time De = $\omega\tau_d$). The linear rheology superimposes in the terminal region for both theory and experiment.
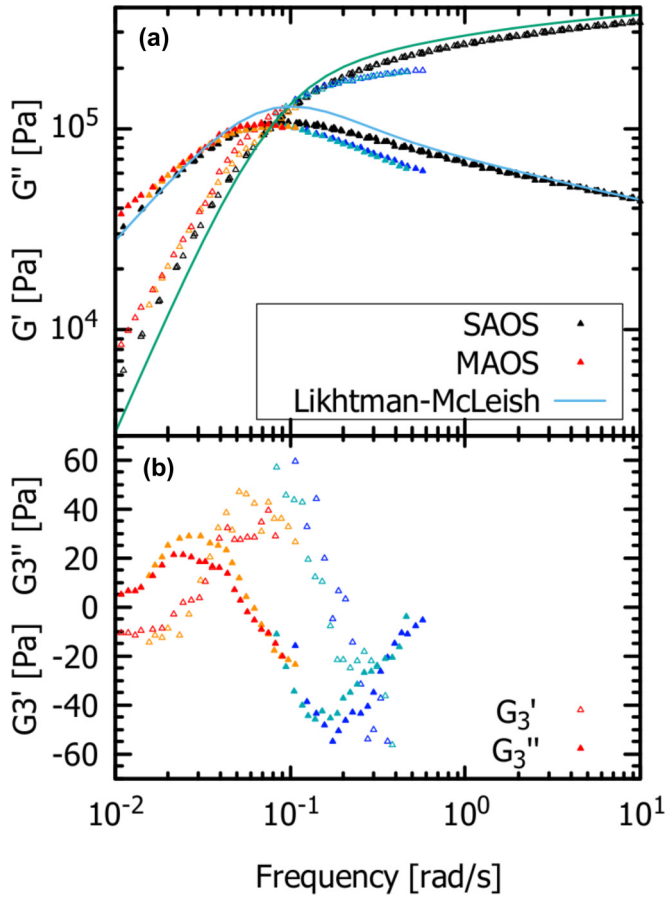
FIG. 7. The linear rheology (a) and LAOS results (b) of PI400k at various temperatures. The predictions of the Likhtman-McLeish model are included: red, 50°, orange, 45°, aqua, 30°, and blue, 25°.

$De = \omega \tau_d$ collapses the terminal linear rheology but not the LAOS features (cf. Fig. 6 in the Appendix). Therefore, LAOS features are associated with faster relaxation processes. The crossover in G'_3 and G''_3 moves to lower De with increasing Mw and further occurs for $De < 1$, hence at lower frequencies than the characteristic reptation rate. All the theories reported here predict the third harmonic crossover to occur at $De > 1$.

To understand these complex rheological structures compared with a nonlinear viscoelastic theory, which simultaneously describes the linear rheology, is essential. This will

(1) test our current understanding of the underlying polymer physics and (2) allow these measurements to be used as an analytical technique.

We now compare the previously introduced molecular rheology theories to the experimental results for the PI100k sample at 25 °C (Fig. 2). We consider the GLaMM model, a one-mode Rolie-Poly (1-RP) model, and a multimode Rolie-Poly (9-RP) model with nine Maxwell modes.

Comparing the linear rheology predicted by Likhtman-McLeish (LM) linear theory which nearly superimposes onto the experimental data in Fig. 1, we see the nonlinear extension of the LM model follows both moduli closely with a slight deviation in G'' near the crossover point. The one-mode RP model is calculated with the moduli and reptation time taken from LM theory and hence captures little of the linear rheology except the correct scaling in the terminal region. Finally, the nine-mode RP model (fitted to experimental data) closely echoes the data over the complete frequency range until the final mode at around 10^5 (rad/s).

In Fig. 3 we compare the nonlinear theories to the LAOS data. We multiplied the modulus of the experimental data by a factor 10 for it be discernible on the plot. While all theories reproduce the qualitative shape of G'_3 and G''_3, it is clear that all theories overestimate the amplitude of the third harmonic by at least a factor 10. It is also clear that the crossover between $G3'$ and $G3''$ occurs at a significantly higher frequency for all theories compared to experiment. We have checked various parameters such as the convective constraint release (CCR) rate, order one parameter (R_s), and the GLaMM discretization (N) which have minor effects on the magnitude of the third harmonics but show no qualitative differences from those presented here (cf. the Appendix). Changing the parameter R_s has the effect of changing the stretch relaxation while preserving the linear rheology. Even changing this parameter (effectually reproducing Fig. 4) cannot bring the third harmonic crossover below a frequency less than τ_d^{-1} and will have the detrimental effect of changing the rheological predictions in transient shear and extensional flows.

We can see in Fig. 4 that there are clear trends in the features of the third harmonics that are a function of molecular weight (or Z). The theory predicts that with greater Z, we see an increase in the magnitude of both the peaks in G'_3 and G''_3 and the negative minima in G''_3, as well as a shift of all features
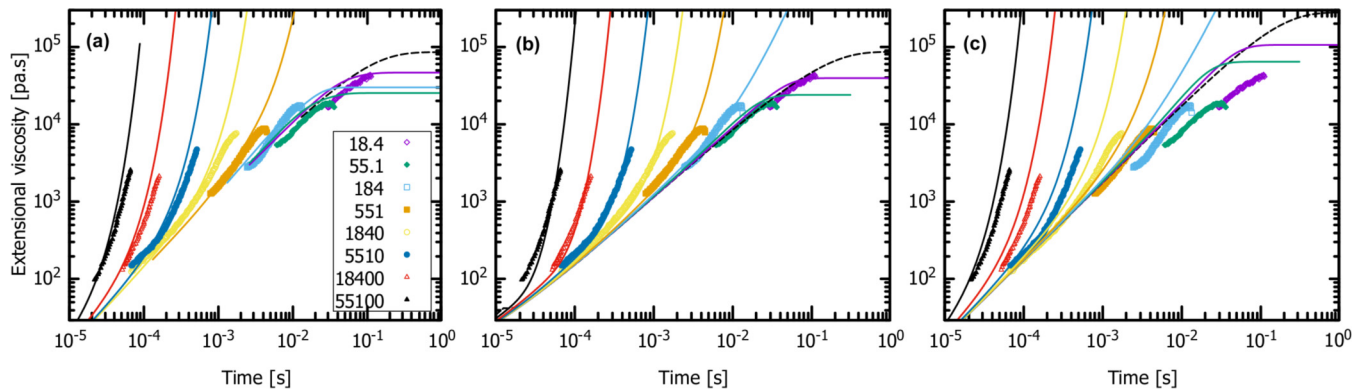

FIG. 8. Extensional rheology measured on a SER attachment at $-30°$. Each subfipanel compares the extensional data to one of the theories used in the main text: (a) GLaMM, (b) nine-mode Rolie-Poly, (c) one-mode Rolie-Poly.
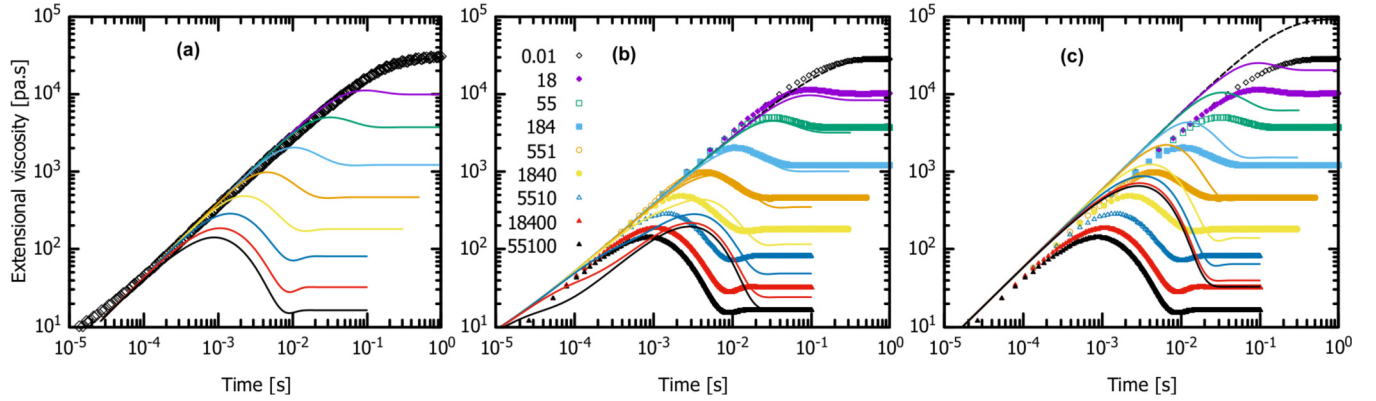
FIG. 9. The shear rheology predictions of the three models used in the main text. (a) The GLaMM model is compared to the linear rheology and the $\eta^*(t)$ envelope can be observed; (b) the nine-mode Rolie-Poly model is compared to GLaMM predictions; and (c) the one-mode Rolie-Poly model is compared to the GLaMM predictions.

to higher De. This is counter to the experimental observations, which show the features moving to lower De with molecular weight (seen in Fig. 6 in the Appendix) and decreasing or remaining as constant magnitude. It is clear, however, that the theories do capture the correct form of the experimental data, capturing all of the features noted in experiment.

Although the single-mode Rolie-Poly model captures little of the linear rheology, it reproduces all the features in the MAOS sweeps, albeit with higher magnitudes. The simplicity of this model means we can extract analytical forms for the real and imaginary components of the third harmonic in the limit of small strain amplitude (given in the Appendix). Although complex, these expressions are dependent only on the oscillation frequency and the Rouse time of the polymer. This implies that the behavior we see, qualitatively captured by this simple model, is driven by chain stretch. This is significant because the frequencies used are well below the inverse Rouse time of the polymers, and so no contribution from Rouse behavior is expected in linear rheology. Moreover, the Rouse behavior of these polymers is difficult to access at all in linear rheological tests. (Here it required temperatures of $-30\,^{\circ}\mathrm{C}$.) MAOS therefore is a tool for probing Rouse behavior at low frequency, which is beneficial for systems where high frequencies are inaccessible, or for semicrystalline

polymers, where TTS is restricted to temperatures above the melting point.

VI. CONCLUSIONS

We report a MAOS protocol alongside evidence that the behavior of polymer melts in MAOS is driven by chain stretch. This method makes polymer chain stretch behavior accessible at low frequencies on standard torsional rheometers.

The standard dynamic moduli for well-entangled polymers ($Z \geqslant 10$) superimpose for Deborah numbers De $\leqslant 10$. The MAOS results show that the samples can be differentiated by probing their weak nonlinear response at De $\lesssim 1$. The MAOS results can differentiate these samples from their nonlinear response, revealing more characteristic properties than linear rheology alone.

The key characteristic flow timescales are the orientation and stretch time (τ_d and τ_r respectively), and these are related to the entanglement time and the number of entanglements. The terminal relaxation crossover allows τ_d to be easily obtained (along with G_e), and determining any of Z, τ_e, or τ_r instantly gives the full rheological map of flow properties. The MAOS measurements clearly access the faster nonlinear relaxation mechanisms, usually measured at De $\gg 1$, at Deborah numbers $O(1)$.
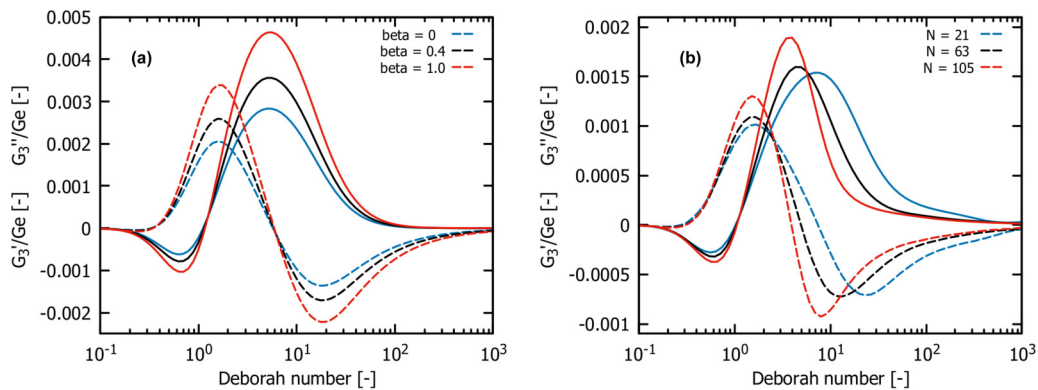
FIG. 10. (a) Variations in the third harmonics as a function of the Rolie-Poly parameter $\beta \in [0, 1]$. The amplitude of features in the third harmonic is shown to increase with increasing β, which parametrizes constraint release. Notice that the crossover does not vary with the amount of CCR. (b) The GLaMM third harmonic predictions shown with different discretization $N = Z, 3Z, 5Z$. Little difference is seen in the GLaMM predictions with increased numerical accuracy.

FIG. 11. Giesekus predictions for PI100k compared to GlaMM, Rolie-poly, and experimental data. The solid lines are G'_3, and the dashed lines are for G''_3'.

An example of the potential of this approach is for semicrystalline polymers where the temperature range accessible in melt rheology is very limited. This restriction is heightened by the often large difference between the glass-transition temperature and the melt-transition temperature, which reduces t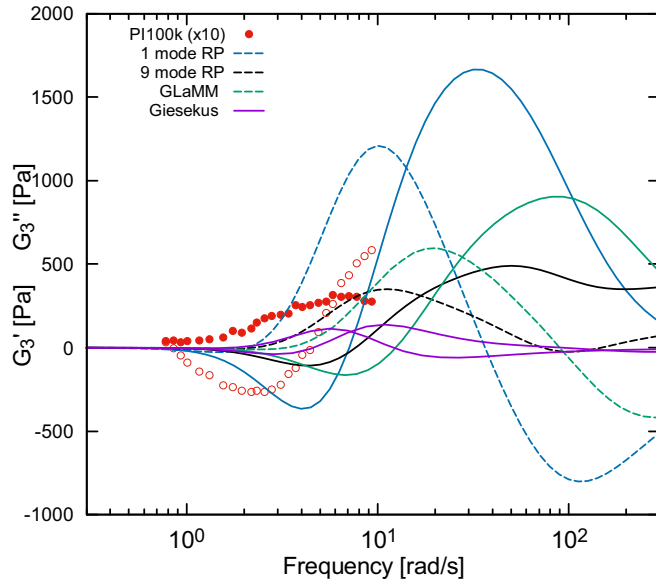he effect of temperature change on viscosity and therefore severely limits the effects of time-temperature superposition theories. However, a modeling approach is required for quantitative study of this behavior, in order to fully establish the complex relationship between this response and the characteristic relation times.

We have shown a significant discrepancy in the predictions of MAOS with Rolie-Poly and GlaMM models, the latter notable for having no adjustable parameters. Qualitatively, the behavior in MAOS is captured by both models, yet remarkably neither quantitatively matches the experimental data for these simple model materials. This indicates an addition

is required, even to the current gold standard in rheological models, to fully capture MAOS data.

APPENDIX

1. Details on sample preparation and measurement protocols

Samples were prepared for rheometry by pressing into disks 1 mm thick and 25 mm in diameter under a force of 4 tonnes at room temperature followed by equilibration for at least 10 minutes. The disk was loaded into the rheometer and the geometry driven to the sample gap $+5\%$. The normal force was left to dissipate to $\leqslant 0.1$N and the sample trimmed after which the geometry was driven to the final sample gap and the normal force again allowed to dissipate before measurement.

Care was taken to ensure the accuracy of the LAOS measurements: (1) many cycles were averaged over (typically 100 plus five startup cycles which were discarded) to minimize the noise in the system (measured using the second harmonic, which should be zero by symmetry [27]), (2) the effects of edge fracture and slip were avoided by monitoring the sample and the magnitudes of the even harmonics and comparison of G' and G'' with the linear rheology, and (3) superharmonic superposition [44] was measured for the instrument and avoided by performing measurements at frequencies under 5 rad/s.

2. Details on constitutive models used

The Likhtman-McLeish linear model [40] was compared to the linear rheology of the PI samples in the main paper. This was not solved directly but using REPTATE software. The following equation was used from the LM model to relate the entanglement time τ_e:

$$\tau_d = 3Z^3 \left(1 - 2\frac{C_1}{\sqrt{Z}} + \frac{C_2}{Z} - \frac{C_3}{Z^{3/2}} \right) \tau_e, \qquad \text{(A1)}$$

where the coefficients are $C_1 = 1.69$, $C_2 = 4.17$, and $C_3 = -1.55$.
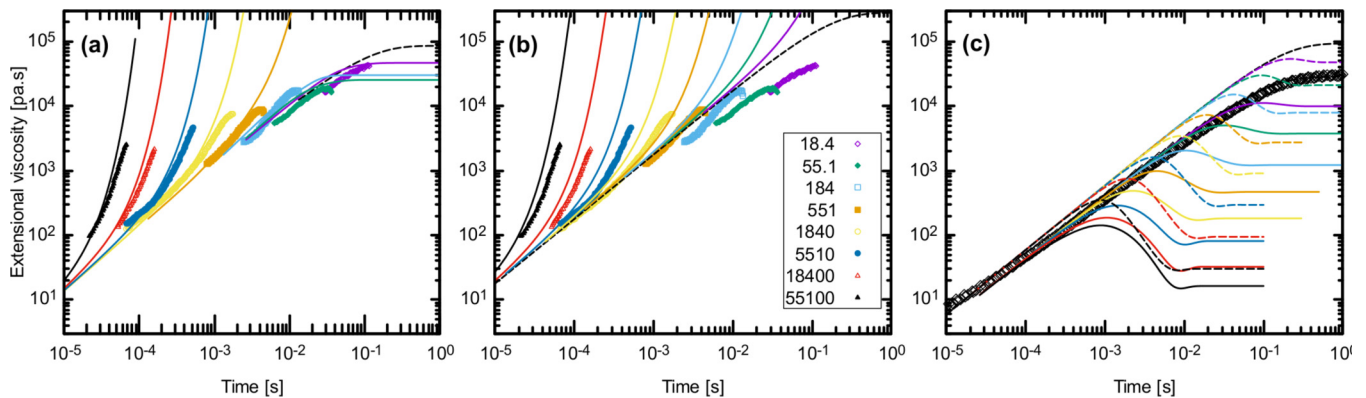
FIG. 12. Comparison of experimental data to the shear and extensional rheology predictions of GlaMM and the Giesekus model with alpha = 0.5, showing that the Giesekus model cannot fit all flows simultaneously with a single value of alpha. (a) Comparison of GlaMM to experimental extension; (b) comparison of Giesekus to experimental extension; and (c) GlaMM (solid lines) and Giesekus (dotted lines) compared to experimental transient shear.

We give an overview of the GLaMM model with full details found in Refs. [41,42]. We calculate the stress tensor as

$$\boldsymbol{\sigma} = \frac{12G_e}{5Z} \int_0^Z \boldsymbol{f}(s, s')\, ds + \frac{G_e}{Z} \int_{-\infty}^t \sum_{p=Z}^N \exp$$

$$\times \left[-\frac{2p^2(t - t')}{Z^2 \tau_e} \right] [\boldsymbol{K}(t') + \boldsymbol{K}(t')^T]\, dt', \quad \text{(A2)}$$

where the first term in the rhs is the stress relaxation at length scales larger than an entanglement and the second term is the

entanglement Rouse relaxation with relaxation time τ_e. G_e is the modulus, Z is the number of entanglements, **K** is the velocity gradient tensor, and p is the Rouse mode number. The $\boldsymbol{f}(s, s')$ tensor is a tangent correlation function,

$$f_{\alpha\beta}(s, s'; t) \equiv \left\langle \frac{\partial R_\alpha(s, t)}{\partial s} \frac{\partial R_\beta(s', t)}{\partial s'} \right\rangle, \quad \text{(A3)}$$

which considers the conformation of the polymer chain described by vector $\mathbf{R}(s, t)$ between points s and s' with $\{s, s'\} \subset [0, Z]$. The evolution of $\boldsymbol{f}(s, s')$ is given by

$$\frac{\partial}{\partial t} f_{\alpha\beta}(s, s'; t) = (\kappa_{\alpha\gamma} f_{\gamma\beta} + f_{\alpha\gamma} \kappa_{\gamma\beta}) + \frac{1}{3\pi^2 Z \tau_e} \left[\frac{Z}{Z^*(t)} \right]^2 \left(\frac{\partial}{\partial s} + \frac{\partial}{\partial s'} \right) \frac{D^*(s, s')}{\lambda(s, s')} \left(\frac{\partial}{\partial s} + \frac{\partial}{\partial s'} \right) f_{\alpha\beta} + \cdots$$

$$+ \frac{3av}{2} \left[\frac{\partial}{\partial s} \frac{1}{\lambda(s)} \frac{\partial}{\partial s} \left(f_{\alpha\beta} - f_{\alpha\beta}^{\text{eq}} \right) + \frac{\partial}{\partial s'} \frac{1}{\lambda(s')} \frac{\partial}{\partial s'} \left(f_{\alpha\beta} - f_{\alpha\beta}^{\text{eq}} \right) \right]$$

$$+ \frac{R_s}{2\pi^2 \tau_e} \left\{ \frac{\partial}{\partial s} \left[f_{\alpha\beta} \frac{\partial}{\partial s} \ln \lambda^2(s) \right] + \frac{\partial}{\partial s'} \left[f_{\alpha\beta} \frac{\partial}{\partial s'} \ln \lambda^2(s') \right] \right\}. \quad \text{(A4)}$$

Equation (A4) contains four terms, which in order are convection, reptation, and contour length fluctuations, constraint release, and retraction. The equation contains parameters for diffusion $[D * (s, s')]$, and a retraction rate $[\lambda(s)]$, with constants for CCR (v) and R_s, a geometric parameter of order unity. By considering the intersegmental motions of the chain in Fourier space, the GLaMM equation can be simplified by considering only the first Fourier mode. This removes the s dependency, and the chain becomes dumbbell-like. The resulting model is the Rolie-Poly model, which is given by

$$\frac{d\boldsymbol{\sigma}}{dt} = \boldsymbol{K} \cdot \boldsymbol{\sigma} + \boldsymbol{\sigma} \cdot \boldsymbol{K}^T - \frac{1}{\tau_d}(\boldsymbol{\sigma} - \boldsymbol{I}) - \frac{2(1 - \sqrt{3/\text{tr}\boldsymbol{\sigma}})}{\tau_r} \left[\boldsymbol{\sigma} + \beta \left(\frac{\text{tr}\boldsymbol{\sigma}}{3} \right)^\delta (\boldsymbol{\sigma} - \boldsymbol{I}) \right]. \quad \text{(A5)}$$

To recover the transient stress growth in both nonlinear shear and extensional flow tests we use the multimode Rolie-Poly model. The faster modes are used to recover the correct viscoelastic envelope (cf. Figs. 8 and 9), and the nonstretch limit of the Rolie-Poly equation is used for these "fast" modes (where stretch is relaxed essentially infinitely fast):

$$\frac{d\boldsymbol{\sigma}}{dt} = \boldsymbol{K} \cdot \boldsymbol{\sigma} + \boldsymbol{\sigma} \cdot \boldsymbol{K}^T - \frac{1}{\tau_d}(\boldsymbol{\sigma} - \boldsymbol{I}) - \frac{2}{3}\text{tr}(\boldsymbol{K} \cdot \boldsymbol{\sigma})[\boldsymbol{\sigma} + \beta(\boldsymbol{\sigma} - \boldsymbol{I})]. \quad \text{(A6)}$$

The simplicity of the Rolie-Poly model [Eq. (A5)] allows some analytic progress to be made. If we expand the (dimensionless) extra stress tensor in increasing powers of strain amplitude we can derive an expression of the Fourier coefficients I_n'' that are applicable in the MAOS regime of flow. More details can be found in Refs. [17,45], where a similar approach was performed on the Pom-pom equations. Formulas for the third harmonics of the Rolie-Poly in limit of small strain amplitude with $\beta = 0$ (and $\tau_d = 1$ for clarity such that each component is dimensionless) are given by

$$I_3' = -\frac{1}{6} \frac{(36\tau_r \omega^6 - 73\tau_r \omega^4 - 39\omega^4 - 35\tau_r \omega^2 - 13\omega^2 + 2\tau_r + 2)\omega^3}{144\omega^{10}\tau_r^2 + 376\omega^8 \tau_r^2 + 72\tau_r \omega^8 + 36\omega^8 + 377\tau_r^2 \omega^6 + 170\tau_r \omega^6 + 85\omega^6 + 123\tau_r 2\omega^4 + 126\tau_r \omega^4 + 63\omega^4 + 19\tau_r^2 \omega^2 + 30\tau_r \omega^2 + 15\omega^2 + \tau^2 + 2\tau_r + 1},$$

$$\text{(A7)}$$

and

$$I_3'' = \frac{1}{6} \frac{(96\tau_r \omega^4 + 8\tau_r \omega^2 + 18\omega^4 - 17\omega^2 - 15\tau_r - 11)\omega^4}{144\omega^{10}\tau_r^2 + 376\omega^8 \tau_r^2 + 72\tau_r \omega^8 + 36\omega^8 + 377\tau_r^2 \omega^6 + 170\tau_r \omega^6 + 85\omega^6 + 123\tau_r 2\omega^4 + 126\tau_r \omega^4 + 63\omega^4 + 19\tau_r^2 \omega^2 + 30\tau_r \omega^2 + 15\omega^2 + \tau^2 + 2\tau_r + 1}.$$

$$\text{(A8)}$$

Indeed, Eqs. (A7) and (A8) give the same result as seen in Fig. 3 for the one-mode Rolie-Poly, i.e., qualitatively similar to the data but quantitatively different in amplitude and frequency dependence. Clearly, the relationship between chain

stretch relaxation time and frequency is complicated and would explain the previous difficultly in extracting molecular information from LAOS.

The parameters used for Likhtman-McLeish and GLaMM theories are shown in Tables II and III, respectively. The other

TABLE II. Likhtman-McLeish theory parameters for polyisoprene at 25 °C that are common to all molecular weights.

G_e	M_e	τ_e	c_v
5.9558×10^5	4.8158	1.321×10^{-5}	0.1

TABLE III. GLaMM theory parameters for simulations.

G_e	τ_d	R_s	c_v
1.0	1.0	2.0	0.1

TABLE IV. One-mode Rolie-Poly Maxwell parameters for PI100k ($Z = 21$) with $\beta = 0$.

G_i	τ_{d_i}	τ_{s_i}
588 844	1.570×10^{-1}	0.0057

TABLE V. Nine-mode Rolie-poly Maxwell parameters for PI100k ($Z = 21$) with $\beta = 0$.

G_i	τ_{d_i}	τ_{s_i}
170 661	1.493×10^{-1}	0.005 628 8
75 449.2	3.316×10^{-2}	–
69 829.9	7.365×10^{-3}	–
52 453.8	1.636×10^{-4}	–
58 903.4	3.632×10^{-4}	–
66 145.8	8.066×10^{-5}	–
154 820	1.791×10^{-5}	–
316 517	3.978×10^{-6}	–
2 103 720	8.834×10^{-7}	–

key parameter for the GLaMM simulations is the entanglement number $Z = \frac{M_w}{M_e}$ from which the entanglement time τ_e is derived from Eq. (A1). We shift the GLaMM results to dimensional numbers using the numbers from Table II and τ_d. In Fig. 5 we plot a comparison of the first and third harmonics as a counterpart to Fig. 4.

The two key observations are (1) that unlike the higher harmonics there is little difference for De < 100 for sufficiently entangled melts, $Z \geqslant 20$ and (2) the crossover between G_3' and G_3'' occurs after the terminal time crossover, which is counter to the experimental observations.

Figure 6 shows the equivalent plot for the experimental data, plotted now against Deborah number. For PI400k we used the Williams-Landel-Ferry (WLF) time-temperature superposition (TTS) theory to increase the total flow regime explored. The results for PI400k depicting the various temperatures are shown in Fig. 7, and these were all shifted to 25 °C to match the data for other molecular weights. It should be noted that GLaMM theory for $Z = 5$ deviates from the behavior of PI20k for De > 1, which is expected since it is a theory for well-entangled melts.

In Fig. 8 we present a comparison between nonlinear extensional experiments and the predictions of the nonlinear constitutive theories used in the main text. We present data for PI100k with measurements taken at -30 °C and TTS shifted to 25 °C. We compare the GLaMM model whose parameters are detailed in Tables II and III, the one-mode Rolie-Poly model (Table IV), and the nine-mode Rolie-Poly model (Table V). The GLaMM model (with no free parameters) and the nine-mode Rolie-Poly model both fit the data excellently. The one-mode Rolie-Poly model captures the strain hardening only at the higher rates. In Fig. 9 we compare the transient shear response of the models. The GLaMM model mimics the linear viscoelastic envelope seen in the extensional data, and in Auhl *et al.* [42] the model is shown to capture nonlinear shear response excellently. The nine-mode Rolie-Poly model compares reasonably to the GLaMM model for intermediate

rates but deviates from the transient response at higher rates. The one-mode model fails to capture nearly every aspect of the GLaMM model other than the general form.

We then show how the third harmonics vary with some model parameters. In the left panel of Fig. 10 we show the Rolie-Poly model (one-mode) for various values of β, the convective constraint release parameter. The magnitude of the third harmonics increases with increasing CCR; however, the frequency dependence is unaffected. The right panel of Fig. 10 compares the GLaMM model for various values of the discretization parameter N, which is an odd multiple of the entanglement number. Overall, there is little difference for different discretization numbers, although the magnitude increase with increasing N and the features move to slightly lower De. The lowest value $N = Z$ matches experiment with the most accuracy. Also, for $N = 105$ simulations took around 3 days per individual frequency to complete and is the practical limit of the simulation time available. For both the above reasons we choose to use $N = Z$ in the main text.

Finally, we include a comparison to a single mode Giesekus [46,47] prediction. Using a value of $\alpha = 0.5$, this gives slightly lower values of G_3' and G_3'' than Rolie-poly and GLaMM (Fig. 11). However, it predicts similar magnitudes for the peaks in G_3' and G_3'', whereas the other models and experimental data show G_3' having a significantly larger peak. Also, crucially, the predictions of transient shear and extensional flows (Fig. 12) are compromised, and it is clear that all three flows cannot be captured by the single nonlinearity parameter in this model.

[1] A. Malmberg, C. Gabriel, T. Steffl, H. Münstedt, and B. Löfgren, Macromolecules **35**, 1038 (2002).

[2] J. F. Vega, A. Santamaria, A. Munoz-Escalona, and P. Lafuente, Macromolecules **31**, 3639 (1998).

[3] J. F. Vega, M. Fernández, and A. Santamaría, A. Muñoz-Escalona, and P. Lafuente, Macromol. Chem. Phys. **200**, 2257 (1999).

[4] R. Zhang, H. Cheng, C. Zhang, T. Sun, X. Dong, and C. C. Han, Macromolecules **41**, 6818 (2008).

[5] K. Hyun, M. Wilhelm, C. O. Klein, K. S. Cho, J. G. Nam, K. H. Ahn, S. J. Lee, R. H. Ewoldt, and G. H. McKinley, Prog. Polym. Sci. **36**, 1697 (2011).

[6] T. S. K. Ng, G. H. McKinley, and R. H. Ewoldt, J. Rheol. **55**, 627 (2011).

[7] L. Martinetti, A. M. Mannion, W. E. Voje, R. Xie, R. H. Ewoldt, L. D. Morgret, F. S. Bates, and C. W. Macosko, J. Rheol. **58**, 821 (2014).

[8] N. A. Bharadwaj, K. S. Schweizer, and R. H. Ewoldt, J. Rheology **61**, 643 (2017).

[9] C. J. Dimitriou, L. Casanellas, T. J. Ober, and G. H. McKinley, Rheol. Acta **51**, 395 (2012).

[10] F. Renou, J. Stellbrink, and G. Petekidis, J. Rheol. **54**, 1219 (2010).

[11] O. C. Duvarci, G. Yazar, and J. L. Kokini, Trends Food Sci. Technol. **60**, 2 (2017).

[12] X. Li, S.-Q. Wang, and X. Wang, J. Rheology **53**, 1255 (2009).

[13] R. H. Ewoldt, A. E. Hosoi, and G. H. McKinley, J. Rheol. **52**, 1427 (2008).

[14] M. A. Cziep, M. Abbasi, M. Heck, L. Arens, and M. Wilhelm, Macromolecules **49**, 3566 (2016).

[15] H. Y. Song, O. S. Nnyigide, R. Salehiyan, and K. Hyun, Polymer **104**, 268 (2016).

[16] M. H. Wagner, V. H. Rolón-Garrido, K. Hyun, and M. Wilhelm, J. Rheol. **55**, 495 (2011).

[17] D. M. Hoyle, D. W. Auhl, O. G. Harlen, V. C. Barroso, M. Wilhelm, and T. C. B. McLeish, J. Rheol. **58**, 969 (2014).

[18] I. Vittorias, M. Parkinson, K. Klimke, B. Debbaut, and M. Wilhelm, Rheol. Acta **46**, 321 (2006).

[19] M. Abbasi, N. Golshan Ebrahimi, and M. Wilhelm, J. Rheol. **57**, 1693 (2013).

[20] N. Clemeur, R. P. G. Rutgers, and B. Debbaut, Rheol. Acta **42**, 217 (2003).

[21] A. Giacomin and J. Oakley, Rheol. Acta **32**, 328 (1993).

[22] R. H. Ewoldt and G. H. McKinley, Rheol. Acta **49**, 213 (2010).

[23] K. S. Cho, K. Hyun, K. H. Ahn, and S. J. Lee, J. Rheol. **49**, 747 (2005).

[24] W. C. MacSporran and R. P. Spiers, Rheol. Acta **23**, 90 (1984).

[25] M. Wilhelm, D. Maring, and H.-W. Spiess, Rheol. Acta **37**, 399 (1998).

[26] M. Wilhelm, P. Reinheimer, and M. Ortseifer, Rheol. Acta **38**, 349 (1999).

[27] M. Wilhelm, Macromol. Mater. Eng. **287**, 83 (2002).

[28] J. G. Nam, K. Hyun, K. H. Ahn, and S. J. Lee, J. Non-Newtonian Fluid Mech. **150**, 1 (2008).

[29] P. K. Singh, J. M. Soulages, and R. H. Ewoldt, J. Rheol. **62**, 277 (2018).

[30] K. Hyun and M. Wilhelm, in *The XV International Congress on Rheology: The Society of Rheology 80th Annual Meeting*, edited by A. Co, G. L. Leal, R. H. Colby, and A. J. Giacomin, AIP Conf. Proc. No. 1027 (AIP, New YorK, 2008).

[31] H. Y. Song and K. Hyun, J. Rheol. **62**, 919 (2018).

[32] H. Y. Song and K. Hyun, Korea-Aust. Rheol. J. **31**, 1 (2019).

[33] O. Carey-De La Torre and R. H. Ewoldt, Korea-Aust. Rheol. J. **30**, 1 (2018).

[34] K. Hyun, E. S. Baik, K. H. Ahn, S. J. Lee, M. Sugimoto, and K. Koyama, J. Rheol. **51**, 1319 (2007).

[35] O. O. Mykhaylyk, C. M. Fernyhough, M. Okura, J. P. A. Fairclough, A. J. Ryan, and R. Graham, Eur. Polym. J. **47**, 447 (2011).

[36] J. D. Ferry, *Viscoelastic Properties of Polymers*, 3rd ed. (John Wiley & Sons, New York, 1987), p. 672.

[37] http://www.reptate.com.

[38] https://sourceforge.net/projects/cdrheo/.

[39] C. D. Reynolds, Ph.D. thesis, Durham University, 2018.

[40] A. E. Likhtman and T. C. B. McLeish, Macromolecules **35**, 6332 (2002).

[41] R. S. Graham, A. E. Likhtman, T. C. B. McLeish, and S. T. Milner, J. Rheol. **47**, 1171 (2003).

[42] D. W. Auhl, J. Ramirez, A. E. Likhtman, P. Chambon, and C. Fernyhough, J. Rheol. **52**, 801 (2008).

[43] A. E. Likhtman and R. S. Graham, J. Non-Newtonian Fluid Mech. **114**, 1 (2003).

[44] A. S. Poulos, F. Renou, A. R. Jacob, N. Koumakis, and G. Petekidis, Rheol. Acta **54**, 715 (2015).

[45] D. M. Hoyle, Ph.D. thesis, University of Leeds, 2010.

[46] A. K. Gurnon and N. J. Wagner, J. Rheol. **56**, 333 (2012).

[47] M. Calin, J. Non-Newtonian Fluid Mech. **165**, 1564 (2010).